9-26-2023

On the Propagation of Whistler-Mode Waves in the 2 Magnetic Ducts

Salman A. Nejad
Embry-Riddle Aeronautical University

Anatoly V. Streltsov
Embry Riddle Aeronautical University, streltsa@erau.edu

Scholarly Commons Citation

Nejad, S. A., & Streltsov, A. V. (2023). On the Propagation of Whistler-Mode Waves in the 2 Magnetic Ducts. *JGR-Space Physics,* (). https://doi.org/10.1029/2023JA031839

On the Propagation of Whistler-Mode Waves in the Magnetic Ducts

Salman A. Nejad[1], **Anatoly V. Streltsov**[1]

[1]Department of Physical Sciences, Embry-Riddle Aeronautical University, Daytona Beach, FL 32114, USA

Key Points:

- MMS satellites observe whistler-mode waves inside the low-magnetic ducts.
- We provide an analytical explanation for the occurrence of leaking ducts and show that the low-magnetic ducts are prone to leak.
- Simulations confirm our analytical prediction of the most trapped whistler-mode waves in the low-magnetic ducts, provided by the least degree of leakage.

Corresponding author: S. A. Nejad, abarghos@my.erau.edu

This article has been accepted for publication and undergone full peer review but has not been through the copyediting, typesetting, pagination and proofreading process, which may lead to differences between this version and the Version of Record. Please cite this article as doi: 10.1029/2023JA031839.

Abstract

This paper studies extremely-low frequency (ELF) whistler-mode waves' behavior within small-scale magnetic field irregularities in the Earth's magnetosphere, known as magnetic ducts. Based on the magnetic fields' magnitude inside and outside these ducts, they are categorized as high-magnetic ducts (HBD) and low-magnetic ducts (LBD). Using the whistler-mode dispersion relation analysis, our primary focus is to show that LBDs are prone to leak electromagnetic energy outside the duct. We further investigate the hypothesis that whistlers can propagate within LBDs without any signal loss when the width of the duct corresponds to an integer multiple of the perpendicular wavelengths of the waves inside it. This condition offers a straightforward and effective method for identifying non-leaking eigenmodes of LBDs. Our analysis of this non-leaking condition reveals that every LBD possesses a finite number of non-leaking eigenmodes directly proportional to the duct's width and the magnitude of the ambient magnetic field within it. The analytical results are then validated using two-dimensional, time-dependent simulations of the electron-Magnetohydrodynamics (EMHD) model. Also, we model the non-leaking propagation of an ELF whistler-mode wave observed inside the LBD by the NASA Magnetospheric Multiscale mission (MMS) satellites.

1 Introduction

Whistler-mode waves have attracted attention from the space plasma community due to their ability to interact with high-energy electrons in the Earth's radiation belt through cyclotron resonance. This interaction changes the pitch angle of energetic particles, causing them to precipitate out of the magnetosphere. By intentionally introducing controlled injections of whistler-mode waves from Earth or space into the magnetosphere, the presence of energetic particles in the Earth's radiation belt can be reduced, thereby creating a safer environment for electronics and crews on space platforms (Inan et al., 1985, 2003).

As a notable characteristic, whistler-mode waves in the magnetosphere propagate along the ambient magnetic field, guided by field-aligned plasma density inhomogeneities referred to as the density ducts, which can be formed as the low-density ducts (LDD) and the high-density ducts (HDD). The presence of these ducts enables the propagation of whistler-mode waves over considerable distances in the Earth's magnetosphere, including from one hemisphere to another, with minimal attenuation.

Recently, (Streltsov & Nejad, 2023) have pointed out the occurrence of small-scale, localized packages of ELF waves within the inhomogeneities of the ambient magnetic field in the equatorial magnetosphere in the data gathered by the NASA Magnetospheric Multiscale Mission (MMS) satellites, which are interpreted as another mechanism of ELF guiding that happens through the magnetic structures, referred to as high-magnetic duct (high-B duct or HBD) and low-magnetic duct (low-B duct or LBD).

For almost 70 years, an extensive study has been done on different density structures, guiding whistler-mode waves in space and laboratory plasmas (Storey, 1954; Nunn, 1974; Karpman et al., 1974; Stenzel, 1976; Omura et al., 1991; Trakhtengerts et al., 1996; Nunn & Smith, 1996; Stenzel, 1999; Hobara et al., 2000; Kostrov et al., 2000; Helliwell, 1965; Sazhin, 1993; Kondrat'ev et al., 1999).

An important feature of density ducts is the ability to guide ELF waves without any leakage for specific conditions. These conditions have been studied in different works. Notably, one of the key findings from these studies is that the leakage of whistler-mode waves from the HDD with very narrow walls can be minimized when the HDD channel encompasses an integer number of the smallest perpendicular wavelengths and the ratio of the largest to the smallest internal perpendicular wavelengths is large (Zaboronkova et al., 1992).

Further studies conducted by (Streltsov et al., 2007; Streltsov, 2007) shed light on the complete elimination of leakage from HDDs with narrow walls, given certain conditions. Specifically, the leakage is entirely eliminated when the width of the duct channel corresponds to an integer multiple of both the smallest and largest perpendicular wavelengths of the internal waves.

Despite the presence of magnetic structures in the inner magnetosphere, the trapping mechanism of ELF whistler-mode waves within them has not been extensively studied. (Yu & Yuan, 2022) investigated the ducting of whistler-mode waves by magnetic dips and peaks by analyzing the wave refractive index. In a recent study, (Streltsov & Nejad, 2023) utilized the whistler-mode dispersion relation to derive analytical criteria for wave trapping in HBD and LBD and to identify thresholds in the magnitude of the ambient magnetic field that facilitates the trapping of waves with specific frequencies. They also determined the ranges of parallel and perpendicular wavelengths of the waves trapped in LBDs and HBDs.

In this study, we examine the leakage from LBDs with narrow walls and investigate the conditions under which the leakage can be entirely eliminated. Specifically, we explore the scenarios where the width of the duct channel corresponds to an integer multiple of both the smallest and largest perpendicular wavelengths of the internal waves. This condition will be further validated through numerical simulations utilizing the full wave model. By conducting these investigations, we will gain a comprehensive understanding of the mechanisms involved in eliminating leakage from LBDs with narrow walls.

2 Observation

Figure 1 shows an event demonstrating a correlation between the wave and the magnetic structure. It consists of the electric field, magnetic field, and plasma density measured by the MMS1 satellite from 19:09:20 to 19:09:40 UT on March 06, 2016. The data are obtained by the MMS1 FPI/DES electron number density, and MMS1 DSP from FIELDS Instrument Suite (Torbert et al., 2016), and magnetic field vector from MMS1 Flux-Gate Magnetometer(FGM) instrument (Russell et al., 2016).

Figure 1a shows with a color pallet the power spectral density (PSD) of the x-component of the electric field (in the GSE coordinate system) in the frequency range $150-330$ Hz and the magnitude of the background magnetic field (white line). Figure 1b shows the corresponding electron density. The minimum magnitude of the ambient magnetic field inside the duct is 33.37 nT (here the electron cyclotron frequency $\omega_{ce} = 5.87\times10^3$ rad/s and the lower hybrid frequency $\omega_{LH} = 1.36 \times 10^2$ rad/s), and it changes during this time interval by $\approx$ 16.91 nT or 50.6% compare to the maximum values outside the duct of 50.28 nT. For comparison, during this time interval, the electron density changes from 83.4 cm^{-3} to 81.9 cm^{-3} or by 1.8%. The density inside the duct is 81.9 cm^{-3} ($\omega_{pe} = 5.1\times10^5$ rad/s). The frequency of the wave in the duct is 248 Hz, and the width of the duct is $\approx$ 13.483 km.

Figure 1c shows the trajectory and the location of MMS satellites in the GSE X-Y plane on March 6, 2016. The red dot indicates the location of MMS satellites at 19:00:00 UT.

In the next section, we present an analytical investigation of the conditions where any LBD with arbitrary values of the duct width and ambient magnetic field guides some whistlers without leakage. Our approach is based on the analysis of the dispersion relation for whistler-mode waves, and it is similar to the analysis of the waveguiding via density ducts developed earlier by (Streltsov et al., 2007; Streltsov, 2007). We also use the same approach and simulations to model an event observed by the MMS1 satellite in Figure 1.

3 Model

The ELF waves ducting in the plasma density inhomogeneities and the magnetic field are investigated by the analysis of the dispersion relation derived from the linearized equations of electron-MHD (EMHD), also called quasi-longitudinal approximation of EMHD, where the displacement current in the Ampere's law is omitted (Helliwell, 1965; Gordeev et al., 1994; Sazhin, 1993). This model is valid for the cases which satisfy the following conditions

$$\omega_{LH} < \omega < \omega_{ce} \ll \omega_{pe}, \tag{1}$$

where, ω_{LH} is the lower hybrid frequency, ω is the angular frequency of the wave; ω_{ce} is the electron gyrofrequency, and ω_{pe} is the electron plasma frequency.

The dispersion relation of ELF-mode waves derived from the quasi-longitudinal EMHD in the homogeneous media is

$$k^2 - \frac{\omega_{ce}}{\omega} k_\parallel k + \frac{1}{\lambda_e^2} = 0 \tag{2}$$

where $k_\parallel$ and $k_\perp$ are parallel and perpendicular to $\mathbf{B}_0$ wavenumber, with $k^2 = k_\parallel^2 + k_\perp^2$, and $\lambda_e = c/\omega_{pe}$ is the electron plasma skin depth.

The relation (2) can be used to express B in terms of $\omega, k_\perp, k_\parallel$, and ω_{pe} in the form of the following function.

$$B = \frac{m_e \omega}{e k_\parallel} \left[\frac{1}{k} \left(k^2 + \frac{1}{\lambda_e^2} \right) \right]. \tag{3}$$

Figure 2 illustrates the meaning of B_1 and B_2, where the plot of B, i.e. equation (3), is depicted as a function of $k_\perp$, $k_\parallel$, and ω_{pe}. It shows that B_1 is the value of the B when $k_\perp = 0$, and B_2 is the minimum value of the B when $k_{\perp_1} = k_{\perp_2}$. Here,

$$B_1 = \frac{m_e}{e} \omega \left(1 + \frac{1}{k_\parallel^2 \lambda_e^2} \right), \tag{4}$$

$$B_2 = \frac{m_e}{e} \omega \left(\frac{2}{k_\parallel \lambda_e} \right). \tag{5}$$

and,

$$k_{\perp_{1,2}} = k_\parallel \left[\frac{\omega_{ce}^2}{4\omega^2} \left(1 \mp \sqrt{1 - \frac{B_2^2}{B^2}} \right)^2 - 1 \right]^{\frac{1}{2}}. \tag{6}$$

Figure 2 reveals another important feature of the LBDs. It shows that for the particular value of ω, there are two different real solutions, $k_{\perp_{1,2}}$, for any B in the range $B_2 < B < B_1$; one real solution outside the duct for $B > B_1$, denoted by $k_{\perp_3}$; and no real solution exists for $B < B_2$.

With all that said above, the ELF wave can propagate inside the LBD if B_I and B_L, the magnetic fields inside and outside the duct respectively, satisfy the following condition.

$$B_2 < B_I < B_1 < B_L. \tag{7}$$

If the magnitude of B inside the channel allows propagation of at least one ELF wave with $B_2 < B$, then for any $B_L > B_1$, there always exists a propagating wave with the same ω and $k_\parallel$ outside the duct. Therefore, the waves inside the duct may couple to the propagating wave outside and carry energy away from the duct, resulting in the leakage of electromagnetic energy from low-B ducts.

The results by (Streltsov et al., 2007) lead to an important condition where the leakage from high-density ducts with thin walls vanishes. Hence, for a duct with a width of $2L$, the leakage is identically zero if

$$\begin{cases} 2L = l\lambda_{\perp_1} \\ 2L = m\lambda_{\perp_2} \end{cases} \quad \text{or} \quad \begin{cases} k_{\perp_1}L = l\pi \\ k_{\perp_2}L = m\pi \end{cases} \tag{8}$$

with both l and m as integer numbers.

Due to the same leaking features, this condition remains valid for the low-B ducts. The following section will study the discrete non-leaking eigenmodes of LBDs.

3.1 Non-leaking Eigenmodes of Low-B Ducts

Following (Streltsov et al., 2007), we introduce dimensionless variables $\Omega = \omega/\omega_{ce}$, $\Omega_p = \omega_{pe}/\omega_{ce}$, $K_\perp = k_\perp c/\omega_{ce}$, and $K_\parallel = k_\parallel c/\omega_{ce}$. In these variables, relation (2) has two solutions for $K_\perp$ as the function of $K_\parallel$, Ω, Ω_p as

$$K_{\perp_{1,2}} = K_\parallel \left[\frac{1}{4\Omega^2} \left(1 \mp \sqrt{1 - \left(\frac{2\Omega\Omega_p}{K_\parallel} \right)^2} \right)^2 - 1 \right]^{\frac{1}{2}}. \tag{9}$$

These two perpendicular wave numbers represent solutions propagating inside the LBD, where the relation (7) is satisfied. Hence, $K_{\perp_{1,2}}$ are real when $K_\parallel$, Ω_p, and Ω satisfy inequalities

$$2\Omega < \frac{K_\parallel}{\Omega_p} < \sqrt{\frac{\Omega}{1-\Omega}}. \tag{10}$$

These inequality relations are the same for HDDs as in (Streltsov, 2007). Figure 3 shows the area satisfying these inequalities.

Applying conditions $K_{\perp_1}L = l\pi$, and $K_{\perp_2}L = m\pi$ to the expressions (9), one gets

$$1 - \sqrt{1 - \left(\frac{2\Omega\Omega_p}{K_\parallel}\right)^2} = 2\Omega\sqrt{\left(\frac{l\pi}{K_\parallel L}\right)^2 + 1}, \tag{11}$$

$$1 + \sqrt{1 - \left(\frac{2\Omega\Omega_p}{K_\parallel}\right)^2} = 2\Omega\sqrt{\left(\frac{m\pi}{K_\parallel L}\right)^2 + 1}. \tag{12}$$

Solutions of the relations (11) and (12) determine families of curves, referred to as l-curves and m-curves, inside the region that is defined by (10). The intersections of these curves provide a finite set of discrete non-leaking eigenmodes of an LBD. Figure 3 shows some of these intersections for specific values of l and m.

4 Simulation

The simulations are based on a quasi-longitudinal electron-MHD model, consisting of equations for the wave electric field, **E**, magnetic field, **B**, and the electron velocity, **v** (Streltsov et al., 2006)

$$\frac{m_e}{\mu_0 n_e e^2}\boldsymbol{\nabla}\times\boldsymbol{\nabla}\times\mathbf{E} + \mathbf{E} = -\frac{m_e}{e}(\mathbf{v}\cdot\boldsymbol{\nabla})\mathbf{v} - \mathbf{v}\times\mathbf{B}, \tag{13}$$

$$\frac{\partial\mathbf{v}}{\partial t} = \frac{1}{\mu_0 n_e e}\boldsymbol{\nabla}\times\boldsymbol{\nabla}\times\mathbf{E}, \tag{14}$$

$$\frac{\partial\mathrm{B}}{\partial t} = -\boldsymbol{\nabla}\times\mathbf{E}. \tag{15}$$

The finite-difference, time-domain (FDTD) technique is employed to numerically implement these equations within a rectangular domain (x, z) (Streltsov et al., 2006). The z-direction aligns with the background magnetic field, while the plasma density and background magnetic fields exhibit homogeneity in the z-direction but inhomogeneity in the x-direction. The domain extends from $-l_z/2$ to $l_z/2$ in the z-direction and from $-l_x/2$ to $l_x/2$ in the x-direction.

The boundary conditions in the z-direction are set to be periodic, with l_z being equivalent to one $\lambda_\parallel$. On the boundaries in the x-direction, the values of **E**, **B**, and **v** are all set to zero, following the Dirichlet boundary conditions. The simulations begin with the initial conditions for **E**, **B**, and **v** as described in (Streltsov et al., 2006).

To solve the Helmholtz equation (13) for **E** at every time step, the method of successive overrelaxation (SOR) is used. A third-order predictor-corrector algorithm is used to advance the equations in time, with the Adamse-Bashforth method as a predictor and the Adamse-Moulton method as a corrector (Streltsov et al., 2006).

4.1 Leaking/Non-leaking Low-B Duct Model

Several numerical experiments were conducted to verify the accuracy of the prediction, which states that leakage from LBD is minimal under conditions (8).

To achieve this goal, we first simulate the propagation of whistler-mode waves within a model LBD with parameters that satisfy the relations (8). Then, we purposely disrupt the non-leaking conditions by modifying the width of the duct in two distinct schemes, e.g., by shrinking and extending the duct size.

In these simulations, we assume that the plasma density remains uniform in the x and z directions, with $n = 60$ cm^{-3}. On the other hand, the magnetic field maintains homogeneous in the z direction while exhibiting inhomogeneity in the x direction. Within the duct, the magnetic field has a magnitude of $B_I = 37.35$ nT, while it measures $B_L =$ 60 nT outside the duct.

The wave frequency is set to $f = 302$ Hz, accompanied by a chosen parallel wavelength of $\lambda_{\|} = 7.298$ km. For these specific wave and plasma parameters, equations (4), (5), and (6) yield the following values: $B_1 = 41.64$ nT, $B_2 = 36.5$ nT, $k_{\perp_1} = 0.79$ rad/km (with $\lambda_{\perp_1} = 7.92$ km), and $k_{\perp_2} = 1.59$ rad/km (with $\lambda_{\perp_2} = 3.94$ km).

To model a non-leaking duct, the initial width of the duct is chosen as $2L = 7.94$ km. This size and the wave parameters calculated above satisfy non-leaking relations $Lk_{\perp_1} = \pi$ (or $2L = \lambda_{\perp_1}$), and $Lk_{\perp_2} = 2\pi$ (or $2L = 4\lambda_{\perp_2}$) inside the channel. To smash the non-leaking case, we repeat the simulation of the same wave two more times by only changing the width of the duct to 60% and 140% of its primary size.

Figure 4 shows the results of the simulations of the three situations mentioned above, accompanied by the propagation of the same wave in the homogeneous background magnetic field. These results show the wave simulations during the time interval of 331 ms or 100 wave periods.

Based on the results presented in Figures 4a, 4b, and 4c, it can be concluded that the wave characterized by the specific values of ω and $\lambda_{\parallel}$ is confined within the LBD, aligning closely with the prediction made using the analytical criteria (7). Figure 4d provides another confirmation for the occurrence of ducting due to the presence of inhomogeneity in the background magnetic field, where in the absence of that inhomogeneity, the same wave propagates at a significant angle relative to the magnetic field.

Figure 4a shows the simulation of the propagation of the whistler-mode wave in the shrunken duct with $2L = 0.6\lambda_{\perp_1}$. The propagation of the whistler-mode wave in the initial duct with $2L = \lambda_{\perp_1}$ is shown in Figure 4b, while the extended duct, for which $2L = 1.4\lambda_{\perp_1}$, is shown in the Figure 4c.

Figures 4a', 4b', and 4c' show profiles of B_0 across $\mathbf{B}_0$ for the shrunken, original, and extended ducts, respectively. Also, the dynamics of $E_x(x, z = 0, t)$ for the shrunken, original, and extended ducts are illustrated respectively in Figures 4a", 4b", and 4c".

The simulations' results in Figure 4 validate the theoretical prediction that leakage from the LBD can be entirely eliminated by ensuring the width of the duct channel aligns with an integer multiple of perpendicular wavelengths of internal waves. This result is evident by comparing the amplitude of E_x component of the propagating wave in Figures 4a", 4b", and 4c", whilst the width of the duct deviates (reduced or extended) form the initial width in Figure 4b', the amplitude of E_x gets smaller, showing that the energy is leaking from the duct.

These simulations highlight the importance of maintaining precise alignment between the channel width and the integer number of perpendicular wavelengths to guide the most trapped wave, as any mismatch between them results in substantial leakage from the duct.

4.2 Leaking/Non-leaking Observed LBD Event

As illustrated in Figure 1, the observed event showcases the confinement of whistler-mode waves within the LBD. In our analysis, we assume that the plasma density and the background magnetic field exhibit homogeneity along the z direction but display inhomogeneity along the x direction. The plasma parameters within the duct are obtained from the observations presented in Figure 1. The wave frequency is 248 Hz. Also, $B_0 = 33.37$ nT, and $n_0 = 81.92$ cm^{-3}, representing the minimum value of the magnetic field inside the duct and the corresponding electron density.

To simulate the observed propagating ELF wave inside the LBD, we need to establish initial conditions by calculating $k_\parallel$ in a way that the wave can be trapped inside the duct. (Williams & Streltsov, 2021) showed that the whistler-mode waves cannot propagate along a high-density duct for every parallel wavelength. Due to the existing similarity between HDDs and LBDs, not all parallel wavelengths will be trapped inside LBDs. For this particular event, $0.903 < k_\parallel < 1.023$ provides two real $k_\perp$s, meaning that the wave may be guided by the duct.

It is also important to note that the approach used to set the simulation parameters for the non-leaking and leaking cases of the event differs from the one employed in simulating the LBD model. In the LBD model, the wave parameters, e.g., $\lambda_\parallel$ and $\lambda_\perp$s, were kept fixed while altering the duct width to create various non-leaking and leaking scenarios using relations (8). However, when dealing with an observed event, it is not admissible to modify the width of the duct. Consequently, the wave parameters are adjusted for the fixed duct width to generate different scenarios for non-leaking and leaking conditions.

- **Wave I**

  To simulate the non-leaking propagation, $k_\parallel$ should be chosen in a way that satisfies the condition (8). This goal will be achieved by choosing $k_\parallel = 0.98$ rad/km ($\lambda_\parallel = 6.89$ km), resulting to $Lk_{\perp_1} = 2\pi$ (or $2L = 2\lambda_{\perp_1}$), and $Lk_{\perp_2} = 3\pi$ (or $2L = 3\lambda_{\perp_2}$) inside the channel.
  Based on this wave and plasma parameters of the event, relations (4), (5), and (6) yield the following values: $B_1 = 39.69$ nT, $B_2 = 33.05$ nT, $k_{\perp_1} = 1.168$ rad/km (with $\lambda_{\perp_1} = 5.38$ km), and $k_{\perp_2} = 1.726$ rad/km (with $\lambda_{\perp_2} = 3.64$ km).

- **Wave II**

  To investigate the leaking situation, we will simulate the wave with the $k_\parallel = 0.925$ rad/km ($\lambda_\parallel = 6.792$ km), resulting in $Lk_{\perp_1} = 1.8\pi$ (or $2L = 1.8\lambda_{\perp_1}$), and $Lk_{\perp_2} = 3.4\pi$ (or $2L = 3.4\lambda_{\perp_2}$) inside the channel. Based on the wave and plasma parameters, $B_1 = 38.83$ nT, $B_2 = 32.59$ nT, $k_{\perp_1} = 1.008$ rad/km (with $\lambda_{\perp_1} = 6.232$ km), and $k_{\perp_2} = 1.901$ rad/km (with $\lambda_{\perp_2} = 3.303$ km).

The outcomes of these simulations, alongside the wave propagation in a homogeneous background magnetic field, are presented in Figure 5. All these results exhibit wave propagation within a time interval of 403 ms or 100 wave periods.

Figure 5 shows that the waves I and II, characterized by the above-mentioned values of ω and $\lambda_{\|}$s, are trapped inside the LBD, following the analytical prediction made by (7). Figure 5c illustrates the dispersion of the whistler-mode wave I in the absence of the magnetic duct.

Figure 5a illustrates the simulation's result of the propagation of a whistler-mode wave I in the duct, satisfying the relations $2L = 2\lambda_{\perp_1}$, and $2L = 3\lambda_{\perp_2}$. On the other hand, Figure 5b presents the simulation's outcome of the propagation of whistler-mode wave II in the same duct, where the relations $2L = 1.8\lambda_{\perp_1}$, and $2L = 3.4\lambda_{\perp_2}$ are satisfied. The Profiles of B_0 across $\mathbf{B}_0$ for these cases are presented in Figures 5a' and 5b', respectively.

By comparing the dynamics of $E_y(x, z = 0, t)$ for the ducts in Figure 5, one can observe the difference between the propagation of the ELF waves in three different situations, i.e., in the presence of the LBD ducts where its width corresponds to an integer multiple of perpendicular wavelengths of the internal wave shown in Figure 5a", in the presence of the LBD ducts where its width does not correspond to an integer multiple of perpendicular wavelengths of the internal wave shown in Figure 5b", and in the absence of the LBD shown in Figure 5c".

5 Conclusions

In this paper, we study the property of LBD to guide whistler-mode waves with minimum attenuation. This is conducted by analyzing the dispersion relation obtained from the linearized equations of the quasi-longitudinal EMHD (Electromagnetic Hydrodynamics) model. Our analysis demonstrates that the low-magnetic duct can leak energy outside due to the potential coupling between the waves propagating inside and outside the duct channel. This property of magnetic ducts is similar to the property of high-density ducts, where they can leak electromagnetic energy due to coupling with the waves outside the channel.

To expand on the earlier studies conducted by (Zaboronkova et al., 1992; Streltsov, 2007) on high-density ducts, our research offers new findings for LBDs. Specifically, we discover that an LBD of a specific width and plasma density can guide a finite number of discrete eigenmodes without experiencing any attenuation.

The central concept explored in this study is the complete elimination of whistler leakage from the LBD by ensuring that the width of the duct aligns with an integer multiple of the perpendicular wavelengths of internal waves. This condition provides a straightforward and efficient method for identifying non-leaking eigenmodes of LBDs.

Finally, by conducting two-dimensional, time-dependent simulations using the complete set of EMHD equations, accounting for the inhomogeneity of the magnetic field of a modeled LBD, we demonstrate that the leak-free condition which is established as an integer ratio between the channel width and the perpendicular wavelength of the wave, allows for the propagation of whistler-mode waves inside the LBD with the least attenuation. Furthermore, we extend our investigation to the propagation of an ELF whistler-mode wave propagating in an observed LBD event.

Acknowledgments

This research was supported by the Air Force Office of Sponsored Research Grants FA9453-322 21-2-0039.

Data Availability

The MMS data used in this study are available from https://lasp.colorado.edu/mms/sdc/public/datasets/ and https://cdaweb.gsfc.nasa.gov/.

The Linux executable code (r1000), data files used to run the code (rbsp_dat_newN.dat and Dens_Bfield_In.dat), and the results from the simulations (ExfieldS.dat) shown in Figures 4 and 5 are available from https://doi.org/10.6084/m9.figshare.c.6835749.v1.

References

Gordeev, A., Kingsep, A., & Rudakov, L. (1994). Electron magnetohydrodynamics. *Physics Reports*, *243*, 215-315.

Helliwell, R. (1965). *Whistlers and related ionospheric phenomena.* Stanford: Stanford University Press.

Hobara, Y., Trakhtengerts, V. Y., Demekhov, A. G., & Hayakawa, M. (2000). Formation of electron beams by interaction of a whistler wave packet with radiation belt electrons. *J. Atmos. Sol.-Terr. Phys.*, *62*, 541.

Inan, U., Bell, T., Bortnik, J., & Albert, J. (2003). Controlled precipitation of radiation belt electrons. *J. Geophys. Res.*, *108*, 1186. doi: 10.1029/2002JA009580

Inan, U., Chang, H., Helliwell, R., Imhof, W., Reagan, J., & Walt, M. (1985). Precipitation of radiation belt electrons by man-made waves: A comparison between theory and measurement. *J. Geophys. Res.*, *90*, 359.

Karpman, V. I., Istomin, Y. N., & Shklyar, D. R. (1974). Nonlinear theory of a quasimonochromatic whistler mode packet in inhomogeneous plasma. *Plasma Phys.*, *16*, 685.

Kondrat'ev, I. G., Kudrin, A. V., & Zaboronkova, T. M. (1999). *Electrodynamics of density ducts in magnetized plasmas.* Amsterdam: Gordon and Breach.

Kostrov, A. V., Kudrin, A. V., Kurina, L. E., Luchinin, G. A., Shaykin, A. A., & Zaboronkova, T. M. (2000). Whistlers in thermally generated ducts with enhanced plasma density: exitation and propagation. *Phys. Scripta*, *62*, 51.

Nunn, D. (1974). A self-consistent theory of triggered vlf emissions. *Planet. Space Sci.*, *22*, 349.

Nunn, D., & Smith, A. J. (1996). Numerical simulations of whistler-triggered vlf emissions observed in antarctica. *J. Geophys. Res.*, *101*, 5261.

Omura, Y., Nunn, D., Matsumoto, H., & Rycroft, M. J. (1991). A review of observational, theoretical and numerical studies of vlf triggered emissions. *J. Atmos. Terr. Phys.*, *53*, 351.

Russell, C. T., Anderson, B. J., Baumjohann, W., & et al. (2016). The magnetospheric multiscale magnetometers. *Space Sci. Rev.*, *199*, 189.

Sazhin, S. (1993). *Whistler-mode waves in a hot plasma.* Cambridge: Cambridge University Press.

Stenzel, R. (1976). Whistler wave propagation in a large magnetoplasma. *Phys. Flu-*

ids, *19*, 857.

Stenzel, R. (1999). Whistler waves in space and laboratory plasma. *L. Geophys. Res.*, *104*, 14379.

Storey, L. (1954). An investigation of whistling atmospheres. *Phil. Trans. Roy. Soc. London, A, 246*, 113.

Streltsov, A. (2007). Spectral properties of high-density ducts. *J. Geophys. Res.*, *112*, A12218. doi: 10.1029/2007JA012710

Streltsov, A., Lampe, M., & Ganguli, G. (2007). Whistler propagation in non-symmetrical density channels. *J. Geophys. Res.*, *112*. doi: 10.1029/2006JAa012093

Streltsov, A., Lampe, M., Manheimer, W., Ganguli, G., & Joyce, G. (2006). Whistler propagation in inhomogeneous plasma. *J. Geophys. Res.*, *111*. doi: 10.1029/2005JA011357

Streltsov, A., & Nejad, S. (2023). Whistler-mode waves in magnetic ducts. *J. Geophys. Res.: Space Phys.*, *128, e2023JA031716*. doi: 10.1029/2023JA031716

Torbert, R.B., Russell, C.T., Magnes, W., & et al. (2016). The fields instrument suite on mms: Scientific objectives, measurements, and data products. *Space Sci. Rev.*, *199*, 105. doi: 10.1007/s11214-014-0109-8

Trakhtengerts, V., Rycroft, M., & Demekhov, A. (1996). Interaction of noise-like and discrete ELF/VLF emissions generated by cyclotron interactions. *J. Geophys. Res.*, *101*, 13293.

Williams, D., & Streltsov, A. (2021). Determining parameters of whistler waves trapped in high-density ducts. *J. Geophys. Res.: Space Phys.*, *126, e2021JA029228*. doi: 10.1029/2021JA029228

Yu, X., & Yuan, Z. (2022). Duct effect of magnetic structures on whistler waves. *J. Geophys. Res.*, *127*. doi: 10.1029/2022JA031013

Zaboronkova, T., Kostrov, A., Kudrin, A., Tikhonov, S., Tronin, A. V., & Shaikin, A. I. (1992). Channeling of waves in the whistler frequency range within nonuniform plasma structures. *Sov. Phys. JETP*, *75*, 625.

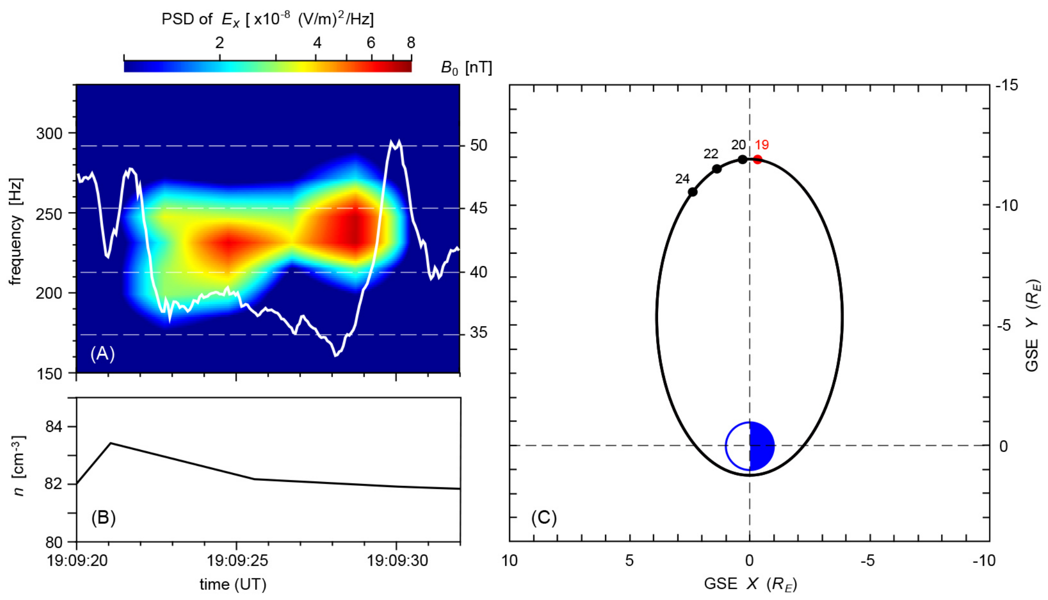

Figure 1. ELF wave packets localized in the low-B duct (LBD) observed by MMS1 satellite on March 06, 2016, from 19:09:20 to 19:09:40 UT. Panel (A) shows the power spectral density (PSD) of E_x component of the electric field in the GSE coordinate system of the satellite (shown with a color pallet) and background magnetic field (shown with the white line). Panel (B) shows the electron density measured by the MMS1 satellite. Panel (C) shows the trajectory and the location of MMS satellites in the GSE X-Y plane on March 6, 2016. The red dot marks the location of the satellites at 19:00 UT.

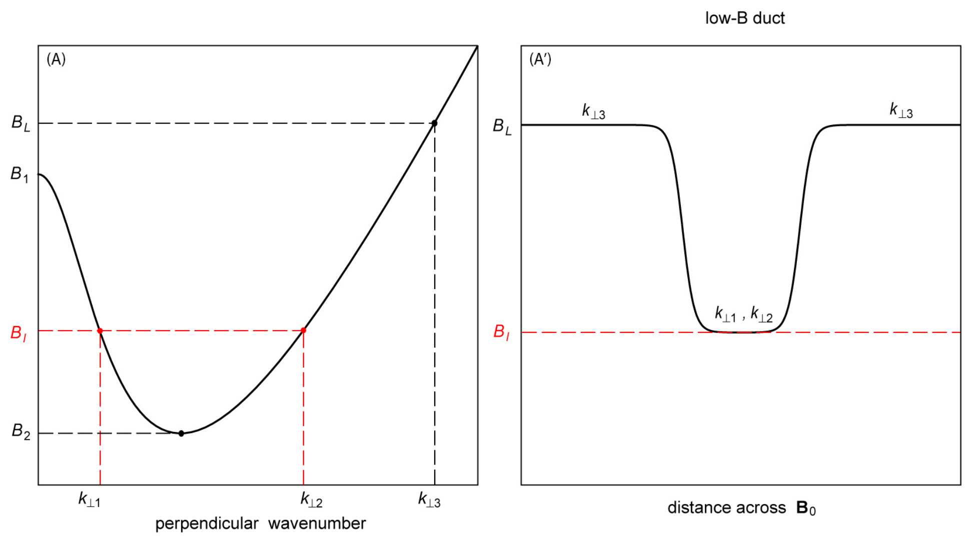

Figure 2. Panel (A): Schematic plot of B as a function of $k_\perp$, ω, $k_\parallel$, and ω_{pe}. Panel (A'): Magnitude of the magnetic field in the direction perpendicular to $\mathbf{B}_0$ corresponding to the low-B duct.

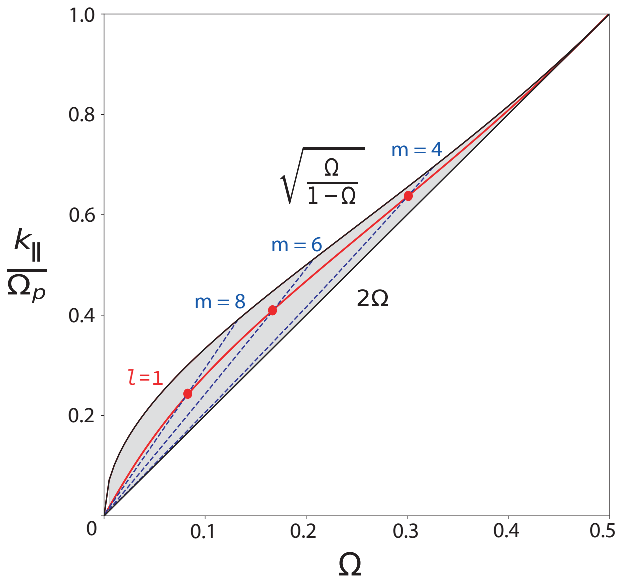

Figure 3. The region in the $(\Omega, K_\parallel, \Omega_p)$ space where real $K_\perp$s exist. The solution of $K_{\perp_1} = l\pi$ for $l = 1$ is plotted by the solid red line, and the solutions of $K_{\perp_2} = m\pi$ are plotted by dashed blue lines for $m = 4, 6$ and 8, when $l = 1$ and $\Omega_p = 10$. Red dots show the intersection of $l = 1$ and $m = (4, 6, 8)$ curves, indicating a set of discrete non-leaking eigenmodes of a low-B duct.

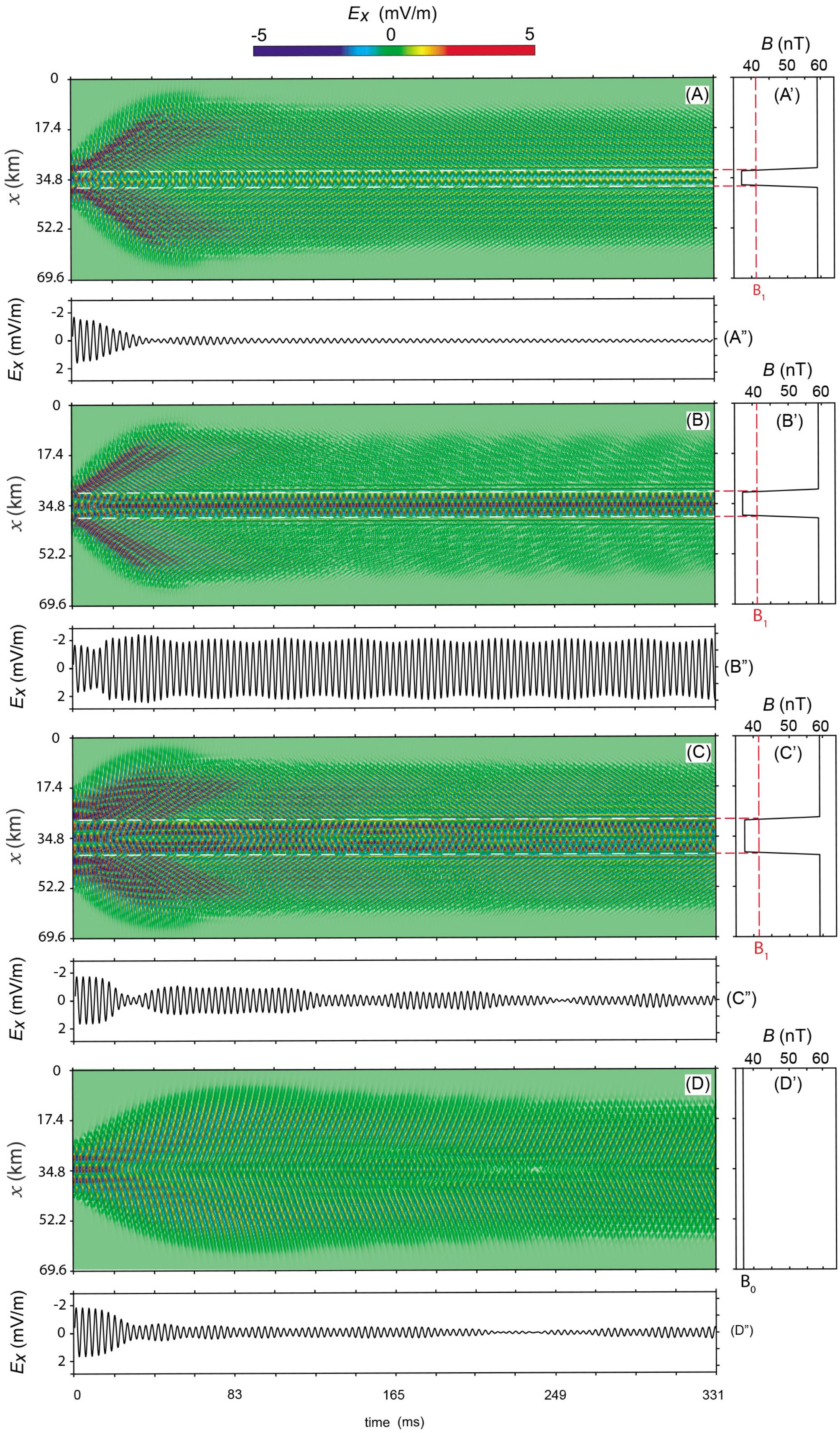

383 **Figure 4.** Continued on the following page.

Figure 4. Panel (A): Dynamics of $E_x(x, z = 0, t)$ in the simulation of the model low-B duct. The wave frequency is $f = 302$ Hz and $\lambda_\parallel = 7.298$ km. Panel (A'): Profile of the magnetic field across $\mathbf{B}_0$. The duct width satisfies $2L = 0.6\ \lambda_{\perp_1}$. Panel (A"): Dynamics of E_x at the center of the computational domain, $E_x(x = 0, z = 0, t)$. Panels (B), (B'), and (B") show the results from the simulations of the same wave with the width satisfying $2L = \lambda_{\perp_1}$. Panels (C), (C'), and (C") show results from the simulations of the same wave with the width satisfying $2L = 1.4\ \lambda_{\perp_1}$. Panels (D), (D'), and (D") show results from the simulations of the same wave with the homogeneous magnetic field, $B_0 = 37.35$ nT.

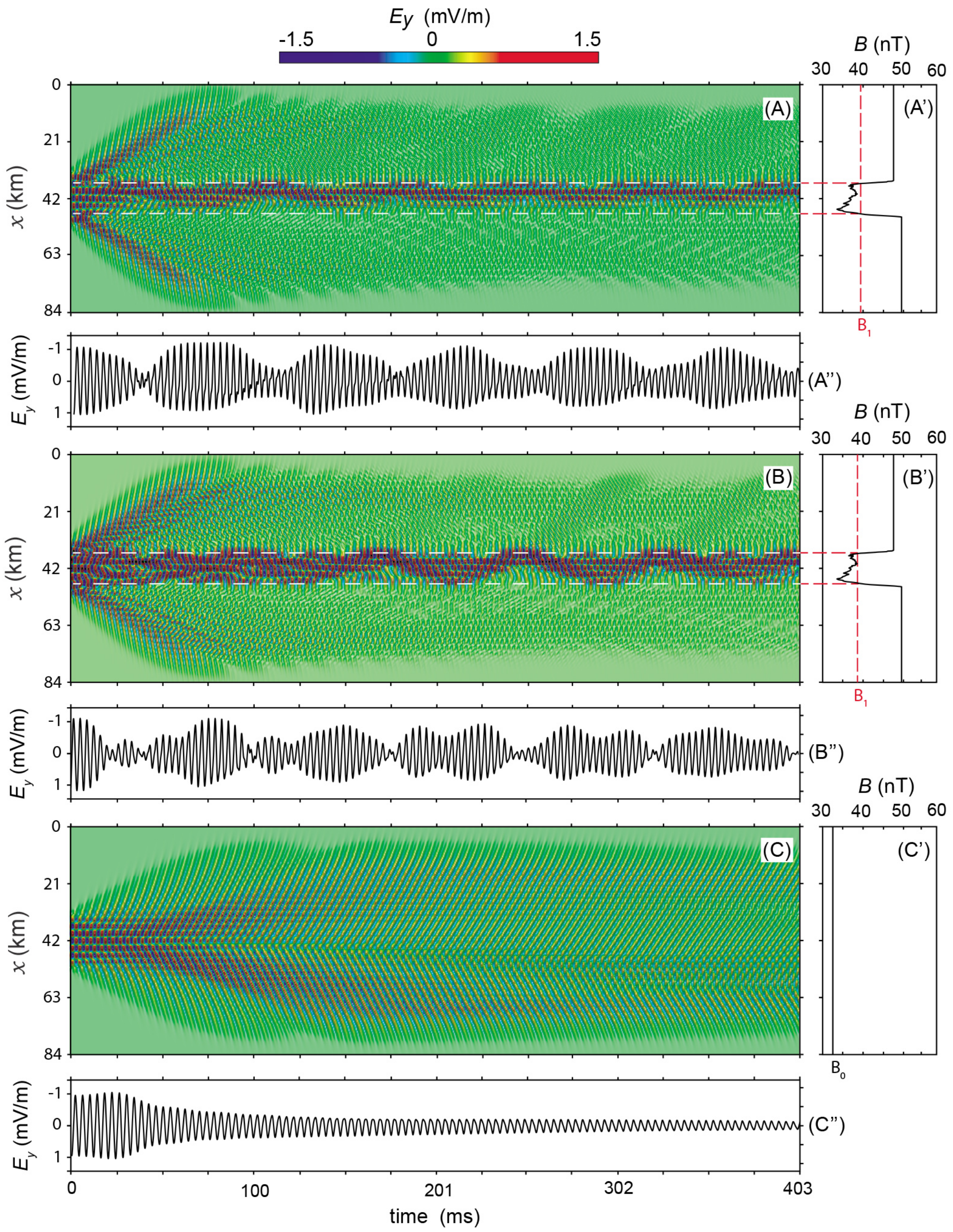

Figure 5. Panel (A): Dynamics of $E_y(x, z = 0, t)$ in the simulation of the observed low-B duct event. The wave frequency is $f = 248$ Hz and $\lambda_\parallel = 6.89$ km. Panel (A'): Profile of the magnetic field across $\mathbf{B}_0$. The width of the duct satisfies $2L = 2\ \lambda_{\perp 1}$. Panel (A"): Dynamics of E_y at the center of the computational domain, $E_y(x = 0, z = 0, t)$. Panels (B), (B'), and (B") show results from the simulations of the wave with the same frequency and $\lambda_\parallel = 6.792$ km, satisfying $2L = 1.8\ \lambda_{\perp 1}$. Panels (C), (C'), and (C") show results from the simulations of the same wave within the panel (A) with the homogeneous magnetic field, $B_0 = 33.37$ nT.